



Source Apportionment and Evolution of N-containing Aerosols at a Rural Cloud Forest in Taiwan by Isotope Analysis

Ting-Yu Chen¹, Chia-Li Chen¹, Yi-Chi Chen², Charles C.-K. Chou³, Haojia Ren^{*,2}, and Hui-Ming Hung^{*,1}

¹Department of Atmospheric Sciences, National Taiwan University, Taipei, 10617 Taiwan

5 ²Department of Geosciences, National Taiwan University, Taipei, 10617 Taiwan

³Research Center of Environmental Changes, Academia Sinica, Taipei, 11529 Taiwan

Correspondence to: Hui-Ming Hung (hmhung@ntu.edu.tw)

Abstract. Ammonium and nitrate are two major N-containing aerosol compositions. The deposition of N-containing aerosols has impacts on regional ecology and the biogeochemical cycle. In this study, aerosols in a rural cloud forest (Xitou in Taiwan) were studied using ¹⁵N and ¹⁸O isotope analysis to assess the sources and formation pathways of the local N-containing aerosols linking to a metropolitan. Aerosol samples were collected for different size ranges using a micro-orifice uniform deposit impactor (MOUDI) on a half-day basis in December 2018. The chemical functional groups were analyzed using a Fourier transformed infrared spectroscopy with attenuated total reflection technique (FTIR-ATR), while the isotope analysis was performed using a gas chromatography-isotope ratio mass spectrometer (GC-IRMS). The average measured aerosol concentration (PM₁₀) was 0.98 (ranging from 0.15 to 3.31) and 0.25 (ranging from 0.00 to 1.51) μg/m³ for NH₄⁺ and NO₃⁻, respectively. In general, a higher functional group concentration was observed during the daytime by a factor of 1.5 to 6 than nighttime, likely due to the transportation of pollutants from upper stream urban and industrial regions through the local sea breeze combined with valley wind. The presence of fog can further elevate the concentration by a factor of 2 to 3, resulting from the stronger inversion and lower boundary layer height. The higher NH₄⁺ concentration in fine particles under foggy conditions can further promote submicron-sized NO₃⁻ formation via aqueous phase dissolution with NH₄⁺ neutralization. Furthermore, the higher RH during fog events shifted the mass distribution of aerosol functional groups to a larger mode size. By comparing the δ¹⁵N value directly or the analysis using a statistical isotope mixing model, MixSIAR, the NH₄⁺ is probably originated from the industries, coal-fired power plants (CFPP), or fertilizer plants, while NO₃⁻ might be contributed from the CFPP, industrial or urban sources. The overall δ¹⁸O of NO₃⁻ is +72.66‰ ± 3.42‰, similar to that in other winter Asia studies, suggesting the major formation pathway via O₃ oxidation (δ¹⁸O = +72.5 to 101.67‰). However, a lower δ¹⁸O (< +67‰) for particles less than 0.56 μm during foggy daytime suggests the local contribution via the peroxy radical oxidation before partitioning into aerosol phase under foggy conditions. Overall, the δ¹⁵N and δ¹⁸O distribution profiles as a function of particle size in the studied rural forest site reveal the evolution of aerosol composition from remote coastal regions with chemical processes along the transport process, which can be further affected by weather conditions such as fog events.

Keywords: aerosol, fog, functional group, nitrogen isotope, oxygen isotope



1 Introduction

Aerosols play an essential role in weather, climate, ecology, and human health (Poschl, 2005; Seinfeld and Pandis, 2006). Aerosols are mainly composed of sulfate, nitrate, ammonium, and other organic species. Nitrogen is one of the significant elements of aerosol in various forms, such as ammonium, nitrate, organic nitrogen, etc. Ammonium and nitrate are the primary N-containing alkaline and acid compositions, respectively, and the balance of the ions can influence aerosol acidity. Also, the local weather, such as fog formation, can be affected by the aerosol characteristics via the hygroscopicity of aerosol composition (Petters and Kreidenweis, 2007). Furthermore, the N-containing aerosols not only affect human health and climate but also play an important role in the regional and global nitrogen biogeochemical cycles. The remote transportation of N-containing aerosols from human activities may result in additional nutrient input at deposition sites, affecting local plant growth and ecology (Bobbink et al., 2010). Therefore, the amount of the N-containing aerosols formed and transported to the rural area and their potential sources should be investigated to evaluate the origin of the N-containing species and their impacts.

Ammonium in aerosols could form from gaseous ammonia, mainly generated from agricultural activities (Behera et al., 2013). Besides, NH_3 from fossil fuel exhaust and slipping during selective catalytic reduction (SCR) processes also contribute to aerosol NH_4^+ formation (Cape et al., 2004). Nitrate in aerosols is produced by oxidation of its precursors, nitrogen oxides (NO_x), emitted from fossil fuel combustion, biomass burning, lightening, and biogenic soil emission. The formation pathway of aerosol NO_3^- varies with conditions. In the daytime, NO can be oxidized by O_3 or peroxy radicals to form NO_2 , which could be photolyzed back to NO or further react with OH radicals to generate nitric acid, forming the nitrate aerosols. At night, NO_2 may further be oxidized to NO_3 , reacting with other NO_2 to form N_2O_5 . The hydrolysis of N_2O_5 gives another pathway to form nitrate aerosols (Jacob, 1999; Seinfeld and Pandis, 2006).

The stable nitrogen isotope in aerosols provides a clue to distinguish the probable sources of nitrogen content. Since the abundance of ^{15}N and ^{14}N in gaseous precursors of NH_4^+ and NO_3^- varies in different emission sources, the $\delta^{15}\text{N}$, defined as $((^{15}\text{N}/^{14}\text{N})_{\text{sample}}/(^{15}\text{N}/^{14}\text{N})_{\text{air}} - 1) \times 1000$ (‰), can act as an indicator of the associated nitrogen species (Felix et al., 2012; Felix et al., 2014; Walters et al., 2015; Pan et al., 2016; Chang et al., 2016; Savard et al., 2017; Pan et al., 2018a; Zhang et al., 2020). For nitrate, not only the $\delta^{15}\text{N}$ can be an index of sources, but the $\delta^{18}\text{O}$, defined as $((^{18}\text{O}/^{16}\text{O})_{\text{sample}}/(^{18}\text{O}/^{16}\text{O})_{\text{VSMOW}} - 1) \times 1000$ (‰), where VSMOW stands for Vienna Standard Mean Ocean Water, can reveal the oxidation pathway (Fig. 1) of nitrate formation due to the $\delta^{18}\text{O}$ difference between its oxidants: O_3 , OH, RO_2 (including hydrogen peroxy and organic peroxy radicals), and H_2O (Hastings et al., 2003; Fang et al., 2011; Gobel et al., 2013).

Xitou, an experimental forest of National Taiwan University, is a planted forest located in central Taiwan. As the origin of Beishih brook, Xitou is in the position of a river valley topography towards the northwest, connecting to Taichung City Metropolitan. Due to the topography, the sea breeze combined with mountain-valley wind dominates the diurnal local circulation, bringing air mass from different regions between daytime and nighttime. During the daytime, the sea breeze combined with valley wind can bring pollutants along the transporting path from coastal areas passing through the coal-fired power plants, industrial sites, and cities. As the wind direction reverses during nighttime, the pollutant concentration decreases



65 (Chen et al., 2021). Besides, the afternoon upslope fog occurs frequently in the Xitou forest due to the boundary layer inversion and the sea breeze combined with valley wind (Hsieh, 2019). Therefore, the fog might affect aqueous chemical processes locally.

The analysis of $\delta^{15}\text{N}$ and $\delta^{18}\text{O}$ for nitrogen-associated species as a function of particle size might provide the origin of the N-containing species and the evolution of transport and chemical processes. This study aims to investigate: 1) the interaction
70 between local circulation and the aerosol composition in a rural forest area linking to a city, 2) how the weather affects the aerosol composition in different sizes, and 3) source apportionment of rural N-containing aerosols by isotopic analysis.

2 Experiment Setup

A field campaign was conducted in Xitou experimental forest (23°40'12" N, 120°47'54" E, 1,179 m a.s.l.) from 1st to 24th
December 2018 to investigate the interaction between air quality, local circulation, and human activities in central Taiwan. To
75 dig into the link between local circulation and aerosol concentration and composition, daytime and nighttime aerosol samples in different sizes were collected using a cascade impactor, and underwent Fourier transformed infrared spectroscopy (FTIR) analysis for the functional group concentration (Coury and Dillner, 2008; Hung et al., 2016). Furthermore, $\delta^{15}\text{N}$ and $\delta^{18}\text{O}$ of N-containing species were measured using the denitrifier method (Sigman et al., 2001; Casciotti et al., 2002). The period mass-averaged $\delta^{15}\text{N}$ values were further analyzed using a mixed stable isotope analysis in R (MixSIAR) model (Stock et al., 2018)
80 to resolve the potential sources of aerosol, while $\delta^{18}\text{O}$ acts as an indicator of the oxidation process for nitrate formation in aerosols.

2.1 Sample collection

Ambient aerosol samples were collected using a 13-stage MOUDI (micro-orifice uniform deposit impactors, Model 125R, MSP Corporation, Shoreview, Minnesota, USA) with 46.2 mm polytetrafluoroethylene (PTFE) membrane filters (Whatman
85 7592-104). The cut-off size of MOUDI was 0.01, 0.018, 0.032, 0.056, 0.1, 0.18, 0.32, 0.56, 1.0, 1.8, 3.2, 5.6 and 10 μm , respectively, and the flow rate of sampling air was 10 L min^{-1} . The samples were categorized into daytime and nighttime to investigate the impact of diurnal mountain/valley-breeze circulation on aerosols. Daytime samples were collected from ~9:00 to ~17:00 (local time), and nighttime samples were from ~18:00 to ~6:00 the next day to represent the valley and mountain breeze, respectively. 20 sets of filter samples were collected from 2nd December 2018 to 22nd December 2018, including 4
90 foggy samples (181207D, 181213N, 181214D, 181215D, YYMMDD Daytime/Nighttime) and 16 non-foggy samples (181202D/N, 181207N, 181208D/N, 181209D/N, 181214N, 181215N, 181216D/N, 181220N, 181221D/N, 181222D/N). The collected filter samples were sealed, covered by aluminum foil, and preserved under 4°C till the laboratory analysis to prevent contaminations.



2.2 FTIR-ATR Analysis

95 The concentrations of functional groups such as NH_4^+ , NO_3^- and SO_4^{2-} were determined via FTIR measurement (Nicolet 6700, Thermo Fisher Scientific, USA) equipped with a single-reflectance attenuated total reflectance (ATR) monolithic diamond accessory (GladiaATR™, PIKE Technologies, USA). Filter samples were pressure-pressed onto the ATR crystal to ensure a closed contact with the crystal. The infrared spectra were scanned at wavenumber from 4000 to 500 cm^{-1} at a resolution of 1 cm^{-1} as shown in Fig. S1. The selected spectrum for a given wavenumber range was fitted with one or multiple Lorentzian
100 curves to derive the peak absorbance (I) of each functional group. The curve fitting function can be written as:

$$A(\nu) = I \times \frac{\sigma^2}{4(\nu - \nu_{\text{peak}})^2 + \sigma^2} \quad (1)$$

where $A(\nu)$ is the distribution of a specific absorption curve, ν is the wavenumber, and σ is the scale parameter (half-width at half-maximum), which is the width of the absorption curve. For a mixture, the observed spectrum is a superposition of each substance i :

$$105 \quad A(\nu, (\nu_{\text{peak},1}, \sigma_1, I_1), (\nu_{\text{peak},2}, \sigma_2, I_2), \dots) = \sum_i A_i(\nu) = \sum_i I_i \times \frac{\sigma_i^2}{4(\nu - \nu_{\text{peak},i})^2 + \sigma_i^2} \quad (2)$$

The analyzing peak was $\sim 1350 \text{ cm}^{-1}$ for nitrate and $\sim 1417 \text{ cm}^{-1}$ for ammonium (Fig. S2); besides, the absorbance peak at $\sim 1080 \text{ cm}^{-1}$ for SO_4^{2-} was applied in a 3-curve fitting because of the nearby absorbance of the PTFE filters (Fig. S3). Therefore, the calibration of absorbance to concentration was based on the former analysis using the correlation of absorbance of FT-IR functional groups to the water-soluble ions measured by ion chromatography (Huang, 2016).

110 2.3 Isotope Analysis

2.3.1 Sample Analysis

Due to the instrumental detection limit, 10 sets of aerosol samples with higher N-containing functional group concentration under distinct weather conditions were selected for $\delta^{15}\text{N}$ and $\delta^{18}\text{O}$ isotope analysis of N-containing species (181202D/N, 181213N, 181214D/N, 181215D, 181220N, 181221D, 181222D, 181222N). Because the isotope analysis requires at least five
115 nmol of equivalent N in less than 5 mL solution (i.e., the molar concentration of $\text{NO}_3 + \text{NH}_4 \geq 1 \mu\text{M N}$), the FTIR measurements provide a quantitative reference to infer the concentration of dissolved N-containing species. If the predicted concentration of one filter was too low, 2 to 4 filters collected on the same day with adjacent size bins were put together in a bottle during the rinsing process to ensure sufficient sensitivity for isotope analysis. Filter samples were cut in half and soaked into 30 mL Milli-Q water (resistivity = 18.2 $\text{M}\Omega$ at 25 °C) and underwent a 30-minute ultrasonication to dissolve the water-soluble ions into the
120 solution. Afterward, the extracted solution was filtered through a 0.22 μm Millipore syringe filter and then preserved in an HDPE bottle. The samples were analyzed for the $\delta^{15}\text{N}$ of total nitrogen (TN) and nitrate + nitrite (NN), and the $\delta^{18}\text{O}$ of NN by the bacterial “denitrifier method” as stated by Sigman et al. (2001), Casciotti et al. (2002), and updated by Weigand et al. (2016). For TN analysis, the oxidation process by adding potassium persulfate in NaOH solution was to oxidize NH_4^+ and



125 other N-containing species in a reduced state into NO_3^- before bacterial digestion. The isotope $^{15}\text{N}/^{14}\text{N}$ and $^{18}\text{O}/^{16}\text{O}$ was measured using a gas chromatography-isotope ratio mass spectrometer (GC-IRMS) composed of a GC column system coupled with Thermo MAT 253 Plus 10 kV IRMS. The international standard IAEA NO3 ($\delta^{15}\text{N} = 4.7 \text{ ‰}$, $\delta^{18}\text{O} = +25.61 \text{ ‰}$) and USGS 34 ($\delta^{15}\text{N} = -1.8 \text{ ‰}$, $\delta^{18}\text{O} = -27.93 \text{ ‰}$) were applied for $\delta^{15}\text{N}$ and $\delta^{18}\text{O}$ calibration (Bohlke et al., 2003). In each batch of measurement, three to five duplicates of standards and bacteria blank were used to ensure the efficiency of bacterial conversion and the stability of mass spectroscopy.

130 Ammonium is a major N-containing component in aerosols as part of TN. Since the concentration of water-soluble TN minus NN correlates well with the measured NH_4^+ concentration from FTIR (Fig. S4), the water-soluble TN-NN can seem as NH_4^+ . Therefore, the $\delta^{15}\text{N}$ of ammonium can be derived by assuming the collected aerosol mainly comprised of nitrate, nitrite, and ammonium with negligible other N forms such as organic nitrogen. The $\delta^{15}\text{N}$ of NH_4^+ can be calculated using Eq. (3) as follows:

$$135 \quad \delta^{15}\text{N}_{\text{NH}_4^+} = \frac{\delta^{15}\text{N}_{\text{TN}} \times M_{\text{TN}} - \delta^{15}\text{N}_{\text{NN}} \times M_{\text{NN}}}{M_{\text{TN}} - M_{\text{NN}}} \quad (3)$$

where M_{TN} and M_{NN} are the molarities of total nitrogen (TN) and nitrate plus nitrite (NN) of the sample solution, respectively. Additionally, since the aerosol nitrite concentration is mostly negligible based on ion-chromatography (IC) analysis of PM_{10} , NN is assumed to be in NO_3^- form, i.e., $\delta^{15}\text{N}$ of $\text{p-NO}_3^- \approx \delta^{15}\text{N}_{\text{NN}}$.

2.3.2 Bayesian Mixing Model Application

140 A Bayesian mixing model, MixSIAR, was applied to assess the contribution of multiple aerosol sources. MixSIAR is a statistical model used to infer the probability of mixture sources by analyzing their tracer composition, such as stable isotope or fatty acids (Stock et al., 2018). In this study, the mass-weighted $\delta^{15}\text{N}$ of NH_4^+ and NO_3^- at each sampling period was used as the observation data. For simplification, the source data adopted the results of Savard et al. (2017) as summarized in Table 1 by assuming that the $\delta^{15}\text{N}$ of NH_4^+ and NO_3^- was directly related to their emission sources, either single source or mixture
145 from those sources. The source data include $\delta^{15}\text{N}$ values from traffic, chemical and metal industries, feedlots, fertilizer plants, and coal-fired power plants (CFPP) for NH_4^+ , and $\delta^{15}\text{N}$ values from traffic, chemical and metal industries, fertilizer plants and oil refinery, and CFPP for NO_3^- nitrogen source apportionment. The gas compressors source was not considered in this study.

3 Results and Discussion

3.1 Functional group concentration by FTIR-ATR

150 The averaged functional group concentration measured using FTIR-ATR of collected 0.01 to 10 μm samples was NH_4^+ : 0.98, NO_3^- : 0.25, SO_4^{2-} : 5.16, and black carbon (BC): 0.81 with the unit of $\mu\text{g}/\text{m}^3$ as summarized in Table 1. The mass concentration distribution of NH_4^+ and NO_3^- as a function of aerosol size is shown in Fig. 2. NH_4^+ is mainly distributed in submicron mode, with the most significant mass concentration in 0.32-0.56 μm . The NO_3^- during the non-foggy period mostly appears in sizes



larger than 1 μm and peaks at 3.2-5.6 μm . The mass distribution pattern of SO_4^{2-} mainly in the sub-micron mode is consistent with that of NH_4^+ (Fig. S5), which suggests that most ammonium is in the form of sulfate-associated salts. On the contrary, NO_3^- in the aerosol is mainly formed from the substitution reaction of sea salt aerosol or dust in the larger size ($> 1 \mu\text{m}$) aerosols by HNO_3 (Evans et al., 2004). The non-observed nitrate in submicron particles during non-foggy days is likely due to the thermodynamic equilibrium under ammonia-limited conditions (Seinfeld and Pandis, 2006). Generally, the functional group concentration was higher for the daytime than that at night (Table 1). Foggy weather also promoted a higher concentration. The influence of weather on the mass concentration distribution is discussed in the following subsections.

3.1.1 Difference between daytime and nighttime

The functional group concentration of NH_4^+ (1.00 $\mu\text{g}/\text{m}^3$) and NO_3^- (0.25 $\mu\text{g}/\text{m}^3$) during non-foggy daytime was higher than that in non-foggy nighttime (0.56 $\mu\text{g}/\text{m}^3$ and 0.04 $\mu\text{g}/\text{m}^3$, respectively) as shown in Table 1, and SO_4^{2-} and BC also have approximately 1.5 times higher concentration during non-foggy daytime. The greater daytime concentration might link to the upstream transportation of urban pollutants by valley wind combining with the sea breeze (Chen et al., 2021). Once the wind direction changes into mountain wind accompanying land breeze, the cleaner upper-stream air diluted the pollutants in the Xitou Forest area.

3.1.2 The Influence of Fog

The daytime concentration of NH_4^+ and NO_3^- was 2 to 4 times higher in the foggy period than that in the non-foggy period (Table 1), and the mass distribution seems to shift to a larger size mode for NH_4^+ as shown in Figs. 2(c) and 2(d). Higher ammonium nitrate concentration might result from the stronger boundary layer inversion on foggy days. When the boundary inversion gets stronger in Xitou area, the moisture transportation by upwelling turbulence is weakened. Therefore, water vapor could accumulate in the lower atmosphere, promoting fog formation and prolonging fog lifetime (Hsieh, 2019). Furthermore, the weakened upward transport could also accumulate pollutants in the lower boundary layer, causing a higher concentration in the ambient atmosphere. The concentration of black carbon (BC) also increased during foggy periods, as shown in Table 1 and Fig. S5. This might reveal the inference of the boundary layer on the higher aerosol concentration because BC is a primary aerosol with limited chemical reactions in the atmosphere.

The mass distribution of NH_4^+ shifted slightly to a larger size mode on foggy days. According to a calculation of simultaneously observed dry and wet aerosol size distribution in Xitou, NH_4^+ -containing aerosol has a hygroscopicity coefficient $\kappa = 0.21 \pm 0.01$ (Chen et al., 2021). The hygroscopic growth of aerosol from averaged RH of 80% under non-foggy circumstances to over 99% during the foggy period could lead to a larger wet aerosol size. Extra high NO_3^- concentration of 0.56-1 μm aerosol was observed during foggy periods accompanied with the high NH_4^+ concentration in that size bin (Fig. 2(d)). In foggy periods, the higher water content of aerosol promotes an aqueous phase reaction of aerosol HNO_3 uptake, and the higher concentration of NH_4^+ , more than $2 \times [\text{SO}_4^{2-}]$, gives extra neutralizing ion to stabilize the NO_3^- as suggested by Chen et al. (2021).



185 3.2 Isotope Analysis of N-containing species

The $\delta^{15}\text{N}$ of NH_4^+ and NO_3^- discussed in this section infers the probable aerosol sources, and the photo-oxidation processes of NO_x in the atmosphere are inferred using measured $\delta^{18}\text{O}$ of NO_3^- . The isotope value of each sample is shown in Fig. 3, and the period mass-weighted averaged $\delta^{15}\text{N}$ and $\delta^{18}\text{O}$ are summarized in Table S1.

3.2.1 $\delta^{15}\text{N}$ of NH_4^+

190 Figure 3(a) shows the $\delta^{15}\text{N}$ value of aerosol NH_4^+ as a function of geometric averaged particle diameter. The $\delta^{15}\text{N}$ varies from -3.70‰ to +21.39‰, and the average mass-weighted $\delta^{15}\text{N}$ value is +11.95‰ with a standard deviation of 2.65‰. The $\delta^{15}\text{N}$ of 0.32-1 μm aerosols is in the range of +7.16‰ to +18.64‰, relatively higher than that of other size bins. The trend of a higher NH_4^+ $\delta^{15}\text{N}$ in submicron aerosols was also observed in Beijing (Pan et al., 2016; Pan et al., 2018b) but was approximately 12‰ lower in general. This offset probably results from the different emission sources or the partitioning processes. Overall, the
195 processes forming aerosol NH_4^+ may lead to the size differentiated $\delta^{15}\text{N}$.

The daytime $\delta^{15}\text{N}$ of NH_4^+ is mostly greater than the nighttime one as summarized in Table 3, likely resulting from the different sources, such as transportation of high- $\delta^{15}\text{N}$ NH_3 from urban rush-hours traffic or industrial sources by sea breeze combined with the valley wind. As the mountain wind dominates after sunset, NH_3 might be attributed to the daytime residual (having lower $\delta^{15}\text{N}$ due to the daytime fractionation) or the local biogenic sources having a lower $\delta^{15}\text{N}$.

200 Fog varies the composition mass distribution among different size bins and can affect the isotopic ratio. Under foggy conditions, especially in foggy daytime, the $\delta^{15}\text{N}$ value of larger size aerosols ($\text{PM}_{1-10}\text{-NH}_4^+$) was higher than non-foggy days and could be up to 21.39‰, similar to that of 0.32-1 μm aerosols. As stated in section 3.1, NH_3 in higher concentrations can promote the partition of HNO_3 during foggy conditions. The larger $\delta^{15}\text{N}$ might result from the hygroscopic particle growth of $\text{PM}_1\text{-NH}_4^+$ with high $\delta^{15}\text{N}$. As NH_4^+ is likely to deliquesce to the liquid phase under high RH conditions, the gas-liquid phase
205 transition could accompany isotope equilibrium fractionation for most aqueous particles (Walters et al., 2018). The NH_3 -rich and high RH conditions might cause the NH_3 partition to condensed phase favors higher $\delta^{15}\text{N}$ during equilibrium fractionation processes (Pan et al., 2018b). On non-foggy days, having a relatively lower composition concentration with more acidic properties (indicating NH_3 limited), a higher portion of NH_3 might participate in the aerosol phase to lead a lower $\delta^{15}\text{N}\text{-NH}_4^+$ toward the original $\delta^{15}\text{N}\text{-NH}_3$.

210 3.2.2 $\delta^{15}\text{N}$ of NO_3^-

The $\delta^{15}\text{N}$ value of NO_3^- as a function of size bin shown in Fig. 3(b) ranges from -1.07 to +6.64‰, with a mass-weighted mean value of +2.98‰ and a standard deviation of 1.20‰. This value agrees with other studies measured in Asia or the Pacific Ocean in winter to spring period (-1‰ \pm 3‰ in spring by Guha et al. (2017); 2.0‰ \pm 0.4‰ in spring and 8.6‰ \pm 0.4‰ in winter by Kim et al. (2019); 3.1 \pm 1.1 ‰ in winter by Kawashima (2019)). Since the mass distribution of NO_3^- different from
215 NH_4^+ and varies under foggy and non-foggy conditions (Fig. 2), the discussion of NO_3^- $\delta^{15}\text{N}$ is then focused on a large mode



PM₁₋₁₀-NO₃⁻ (1 μm < geometric diameter < 10 μm) and a small mode PM₁-NO₃⁻ (< 1 μm) particles separately. PM₁₋₁₀-NO₃⁻ is available for most samples, but PM₁-NO₃⁻ is limited to foggy daytime due to the available alkaline species as stated in section 3.1.2. For a given sampling period, PM₁-NO₃⁻ has lower δ¹⁵N (-1.07 to +3.19‰) than PM₁₋₁₀-NO₃⁻ (+1.85 and +6.64‰), likely due to different formation processes. PM₁₋₁₀-NO₃⁻ might be formed through the reaction of HNO₃ or NO₂ with the coarse
220 particles composing NaCl or dust (Evans et al., 2004; Hoffman et al., 2004) during the transport from the coast through the urban region and further to Xitou. Therefore, a higher δ¹⁵N NO₃⁻ participates in the aerosol-phase through isotopic equilibrium fractionation with lower δ¹⁵N HNO_{3(g)} or NO₂ gas molecules remaining in the air (Walters and Michalski, 2015). In contrast, PM₁-NO₃⁻ only occurs in the foggy days, likely forming in the mountain region with high water content and available NH₃. The available HNO_{3(g)} for PM₁ is from the residual NO_x (after reacting with coarse mode particles at the upper stream) and has
225 lower δ¹⁵N compared to PM₁₋₁₀-NO₃⁻. The PM₁-NO₃⁻ formed through the aqueous phase reaction under high NH₄⁺ with effective gas-phase NO₂ uptake might have a limited isotopic selection which leads to a low δ¹⁵N of NO₃⁻ under foggy conditions.

The sample of 21D is a special case with higher δ¹⁵N values. It might result from the agricultural activities nearby, including fertilizing and mowing. The fertilizer generates NO_x with higher δ¹⁵N (Savard et al., 2017), which indicates that the agricultural
230 activities might cause higher δ¹⁵N values than other days.

3.2.3 δ¹⁸O of NO₃⁻

The δ¹⁸O of NO₃⁻ ranged from +53.90 to +79.81‰ (Fig. 3(c)), with a half-day period mass-weighted average of +72.66‰ and a standard deviation of 3.42‰. The results are within the δ¹⁸O range observed in cool seasons over the Mt. Lulin site in Taiwan (69‰ ± 15‰ reported by Guha et al. (2017)) and also in the typical range of other studies (averaged value from 70.9‰ to 83.8
235 ‰) (Savarino et al., 2007; Wankel et al., 2010; Fan et al., 2020; Sun et al., 2020). The relatively high δ¹⁸O compared to summer samples (32 ± 13‰ reported by Guha et al. (2017)) indicates that most NO₃⁻ precursors (i.e., NO_x) were formed by O₃ oxidation whether it was further oxidized through OH oxidation of NO₂ or N₂O₅ hydrolysis pathways (from +72.5‰ to +101.67‰, detailed in SI description). The slightly lower daytime δ¹⁸O (+69.67‰ to +72.52‰ based on half-day average) compared to nighttime samples (+74.82‰ to +79.81‰) as shown in Table S1 indicates that peroxy radicals might partially participate in
240 the daytime photooxidation processes or relatively lower δ¹⁸O of OH leading to a lower δ¹⁸O in nitrate aerosols during daytime as stated in other studies (Gobel et al., 2013; Hastings et al., 2003; Fang et al., 2011).

For PM₁, the δ¹⁸O of 0.32-0.56 μm NO₃⁻ under foggy conditions (+53.90‰ and +66.13‰ for 14th December and 15th December daytime sample, respectively) is relatively lower than that over larger sizes (e.g., +75.65‰ and +73.98 ‰ of 0.56-1 μm) suggesting the formation pathway difference. The concentration of 0.32-0.56 μm NO₃⁻ is relatively lower than that of 0.56-1
245 μm or PM₁₋₁₀, and it might attribute to ambient air mass nearby the observation site. Because the fine particles are more acidic (Chen et al., 2021), NO₃⁻ can frequently exchange with gas-phase HNO₃ to reveal the local δ¹⁸O of NO₃⁻. The peroxy radicals derived from the biogenic volatile organic compounds photooxidation at Xitou forest area might be active oxidants locally for fine mode organic nitrate (RONO₂ or ROONO₂) and HNO₃ from NO + RO₂ → NO₂ + RO and NO₂ + OH → HNO₃ oxidation



to have a lower $\delta^{18}\text{O}$ of NO_3^- (SI description). On the other hand, the higher $\delta^{18}\text{O}$ of $0.56\text{-}1\ \mu\text{m}\ \text{NO}_3^-$ is likely formed from the
250 growth of smaller particles and aqueous phase reactions such as HNO_3 partition, which could be neutralized by excess NH_4^+
at an earlier stage to be less influenced by peroxy radicals. Furthermore, the $\text{PM}_{1-10}\text{-NO}_3^-$ are mainly produced nearby the
urban regions via the reactions of HNO_3 or NO_x with sea salt, i.e., $\text{HNO}_3 + \text{NaCl}_{(\text{p})} \rightarrow \text{HCl}_{(\text{g})} + \text{NaNO}_{3(\text{p})}$ or $2\text{NO}_2 + \text{NaX}_{(\text{p})} \rightarrow$
 $\text{XNO}_{(\text{g})} + \text{NaNO}_{3(\text{p})}$ ($\text{X} = \text{Cl}$ or Br), which may also produce NO_3^- with a higher $\delta^{18}\text{O}$ because most O atoms of NO_3^- can come
from O_3 during the fast $\text{NO} \leftrightarrow \text{NO}_2$ conversion processes (Gobel et al., 2013).

255 3.3 Source apportionment by isotope analysis

The $\delta^{15}\text{N}$ of collected NH_4^+ and NO_3^- is applied for source apportionment since $\delta^{15}\text{N}$ in N-containing aerosol is dependent on
the precursor sources (Felix and Elliott, 2014; Walters et al., 2015; Chang et al., 2016; Pan et al., 2016; Savard et al., 2017;
Pan et al., 2018b; Fan et al., 2019). Figure 4 shows the averaged $\delta^{15}\text{N}$ under distinct weather conditions and the isotope value
of single-source based on the observation by Sarvard et al. (2017). By assuming that the mass-weighted average isotope
260 represents the possible source contribution with a single source having similar $\delta^{15}\text{N}$ as reported by Sarvard et al. (2017) for
simplification, the probable aerosol-N sources are summarized in Table 3. NH_4^+ might be originated from CFPP, traffic, or
industries and least likely from feedlots. The urban sources or CFPP might contribute to $\text{PM}_{1-10}\text{-NO}_3^-$, and industries to the
lower $\delta^{15}\text{N}$ of $\text{PM}_1\text{-NO}_3^-$ under foggy conditions. In contrast, the significant difference of $\delta^{15}\text{N}$ between measurement and
fertilizer plants (+10.8‰) suggests the limited contribution of fertilizer production-related NO_3^- . Overall, the probable sources
265 of NH_4^+ and NO_3^- were anthropogenically originated, such as CFPP, industries, and urban traffic. The sea breeze could
transport the precursor gases or aerosol phase pollutants from coastal coal-fired power plants, industrial sources, or urban
emissions to the forest area by upslope wind (Chen et al., 2021). During the transportation, the chemical reactions might further
promote PM formation, having the measured $\delta^{15}\text{N}$ of collected samples close to that of the available gas-phase species.

As PM is a mixture attributed from various sources, the weight-averaged half-day $\delta^{15}\text{N}$ of NH_4^+ and NO_3^- was analyzed using
270 the MixSIAR model to distinguish the posterior probability of aerosol sources as summarized in Table 4. The daytime samples
of 21st December were excluded in this analysis due to the interference from the agricultural activities nearby. With taking
account of all weather conditions, the order of the possible sources from the highest to the lowest probability is {industries,
CFPP, fertilizers, traffic, feedlots}. The first two sources have a higher likelihood, > 20%. As the conditions were divided with
different weather patterns, fertilizer plants have increased the importance, especially for foggy daytime. Feedlots remain the
275 lowest. The model results agree with the direct comparison, indicating that the anthropogenic sources contribute significantly
to aerosol- NH_4^+ . The larger $\delta^{15}\text{N}$ during foggy daytime suggests a higher probability from fertilizer production, indicating the
likelihood of locally produced ammonium from the fertilizer manufacturers nearby the agricultural area because of the lower
wind speed and lower boundary layer height.

Though the $\delta^{15}\text{N}$ of NO_3^- might seem similar and have no difference between each other, some trends could be revealed from
280 the MixSIAR model analysis. The MixSIAR results show that industries, urban, and CFPP are the major sources for both
 $\text{PM}_1\text{-NO}_3^-$ and $\text{PM}_{1-10}\text{-NO}_3^-$, whereas fertilizer plants have the lowest probability. The posterior probability of PM_1 and PM_{1-10}



nitrate sources has difference slightly: the $PM_{1-10} NO_3^-$ was more likely from CFPP or urban sources, while industries took the majority of $PM_1-NO_3^-$ formation. The inferred source difference might suggest that the coarse mode aerosols came from the coastal sea salt particles mixing with the emission of coal-fired power plants or the Taichung-Changhua metropolitan during the inland transportation. On the other hand, $PM_1-NO_3^-$ is likely formed locally and might have a higher portion of nearby sources. For both PM_1 and PM_{1-10} nitrate, fertilizer industry was the minority of the NO_3^- sources in the Xitou forest area in this study, which is different from the result of NH_4^+ . The discrepancy might result from the type of produced nitrogen fertilizers in the nearby area or the higher contribution of NO_3^- from the power plant or urban sources through sea breeze and valley wind transport.

290 4 Conclusions

The mass distribution of aerosol NH_4^+ and NO_3^- concentration and the associated isotope analysis were analyzed to investigate the evolution of nitrogen species before reaching the studied site. In Xitou forest, the average concentration of aerosol composition is $0.98 \mu\text{g}/\text{m}^3$ for NH_4^+ and $0.25 \mu\text{g}/\text{m}^3$ for NO_3^- . The 1.5 to 6 times higher concentration of NH_4^+ and NO_3^- in the daytime indicates the local circulation combining land-sea breeze with mountain-valley wind could bring urban and industrial pollutants into the Xitou forests, further proved by the $\delta^{15}\text{N}$ analysis. The $\delta^{15}\text{N}$ of NH_4^+ from -3.70‰ to $+21.39\text{‰}$ with higher NH_4^+ $\delta^{15}\text{N}$ values of the $0.32\text{-}1 \mu\text{m}$ aerosols, where a higher concentration was measured, indicates that the aerosol was probably from the anthropogenic contribution by directly comparing with other studies or using the MixSIAR model. The $\delta^{15}\text{N}$ of NO_3^- was from -1.07 to $+6.64\text{‰}$, with a mean value of 2.98‰ and a standard deviation of 1.20‰ . Though the similar range of NO_3^- among sources made it difficult to distinguish the origin of NO_3^- directly, the statistical model still provided some hints: Industries, urban, and CFPP are the significant sources of particulate NO_3^- . The stronger boundary layer inversion during foggy days led to weaker upward transportation of air mass, causing a 2-3 times higher aerosol concentration. The mass distribution difference and the discrepancy of $\delta^{15}\text{N}$ of NO_3^- between foggy and non-foggy conditions suggest that the additional $PM_1-NO_3^-$ for foggy days was formed locally with excess NH_3 in the aqueous phase. The difference of analyzed nitrogen sources between PM_{1-10} and $PM_1 NO_3^-$ revealed the impacts of fog on aerosol formation: PM_{1-10} was more likely produced by CFPP and urban area, whereas PM_1 , only existed in the foggy period, had more local contributors such as a higher portion of industries. The inferred source difference might suggest that the N atoms of coarse mode aerosols came from the coastal sea salt particles mixing with the emission of coal-fired power plants or the Taichung-Changhua metropolitan during the inland transportation. On the other hand, $PM_1-NO_3^-$ is likely formed locally and might have a higher portion of nitrogen from nearby sources. However, the fractionation during the aerosol transportation under higher RH and high gaseous precursors can enlarge the isotope value in aerosol phases (Chang et al., 2018), which might affect the source apportionment results and should be appropriately assessed in the future. The observed $\delta^{18}\text{O}$ of NO_3^- in this study, consistent with former studies conducted in a similar season, suggests that O_3 is the primary oxidant for NO_x as a precursor of NO_3^- . The lower $\delta^{18}\text{O}$ value at $0.32\text{-}0.56 \mu\text{m}$ NO_3^- under foggy daytime conditions indicates the participation of locally produced RO_2 in NO_3^- formation. Overall, the



measured composition combined with the weather observation indicates the effects of local circulation and boundary layer on
315 air quality, and the isotope analysis further proved the influence of the inland transport from anthropogenic sources.

Author contributions

TY Chen and CL Chen carried out the field studies and aerosol composition analysis. TY Chen performed data analysis and
MixSIAR model for N source apportionment and prepared the manuscript draft and editing. YC Chen and H Ren developed
and conducted the isotope analysis. CCK Chou provides MOUDI instrumentation support and IC analysis of PM_{2.5} and PM₁₀.
320 HM Hung supervised the project, including data discussion and manuscript editing.

Competing interests

The authors declare that they have no conflict of interest.

Acknowledgments

This study is supported by the Ministry of Science and Technology, Taiwan (108-2111-M-002-003, 109-2111-M-002-003,
325 and 110-2111-M-002-010) and National Taiwan University (110L892001). We acknowledge the local site support from the
Administration of the Xitou Experimental Forest, College of Bio-Resources and Agriculture at National Taiwan University.

References

- Behera, S. N., Sharma, M., Aneja, V. P., and Balasubramanian, R.: Ammonia in the atmosphere: a review on emission sources,
atmospheric chemistry and deposition on terrestrial bodies, *Environ Sci Pollut Res Int*, 20, 8092-8131, 10.1007/s11356-013-
330 2051-9, 2013.
- Bobbink, R., Hicks, K., Galloway, J., Spranger, T., Alkemade, R., Ashmore, M., Bustamante, M., Cinderby, S., Davidson, E.,
Dentener, F., Emmett, B., Erisman, J. W., Fenn, M., Gilliam, F., Nordin, A., Pardo, L., and De Vries, W.: Global assessment
of nitrogen deposition effects on terrestrial plant diversity: a synthesis, *Ecological Applications*, 20, 30-59, 10.1890/08-1140.1,
2010.
- 335 Bohlke, J. K., Mroczkowski, S. J., and Coplen, T. B.: Oxygen isotopes in nitrate: new reference materials for ¹⁸O:¹⁷O:¹⁶O
measurements and observations on nitrate-water equilibration, *Rapid Commun Mass Spectrom*, 17, 1835-1846,
10.1002/rcm.1123, 2003.
- Cape, J. N., Tang, Y. S., van Dijk, N., Love, L., Sutton, M. A., and Palmer, S. C.: Concentrations of ammonia and nitrogen
dioxide at roadside verges, and their contribution to nitrogen deposition, *Environ Pollut*, 132, 469-478,
340 10.1016/j.envpol.2004.05.009, 2004.



- Casciotti, K. L., Sigman, D. M., Hastings, M. G., Bohlke, J. K., and Hilkert, A.: Measurement of the oxygen isotopic composition of nitrate in seawater and freshwater using the denitrifier method, *Analytical Chemistry*, 74, 4905-4912, 10.1021/ac020113w, 2002.
- Chang, Y., Liu, X., Deng, C., Dore, A. J., and Zhuang, G.: Source apportionment of atmospheric ammonia before, during, and
345 after the 2014 APEC summit in Beijing using stable nitrogen isotope signatures, *Atmospheric Chemistry and Physics*, 16, 11635-11647, 10.5194/acp-16-11635-2016, 2016.
- Chang, Y., Zhang, Y., Tian, C., Zhang, S., Ma, X., Cao, F., Liu, X., Zhang, W., Kuhn, T., and Lehmann, M. F.: Nitrogen isotope fractionation during gas-to-particle conversion of NO_x to NO_3^- in the atmosphere – implications for isotope-based NO_x source apportionment, *Atmospheric Chemistry and Physics*, 18, 11647-11661, 10.5194/acp-18-11647-2018, 2018.
- 350 Chen, C.-L., Chen, T.-Y., Hung, H.-M., Tsai, P.-W., Chou, C. C. K., and Chen, W.-N.: The influence of upslope fog on hygroscopicity and chemical composition of aerosols at a forest site in Taiwan, *Atmospheric Environment*, 246, 10.1016/j.atmosenv.2020.118150, 2021.
- Coury, C. and Dillner, A. M.: A method to quantify organic functional groups and inorganic compounds in ambient aerosols using attenuated total reflectance FTIR spectroscopy and multivariate chemometric techniques, *Atmospheric Environment*,
355 42, 5923-5932, 10.1016/j.atmosenv.2008.03.026, 2008.
- Evans, M. C., Campbell, S. W., Bhethanabotla, V., and Poor, N. D.: Effect of sea salt and calcium carbonate interactions with nitric acid on the direct dry deposition of nitrogen to Tampa Bay, Florida, *Atmospheric Environment*, 38, 4847-4858, 10.1016/j.atmosenv.2004.05.046, 2004.
- Fan, M.-Y., Zhang, Y.-L., Lin, Y.-C., Chang, Y.-H., Cao, F., Zhang, W.-Q., Hu, Y.-B., Bao, M.-Y., Liu, X.-Y., Zhai, X.-Y.,
360 Lin, X., Zhao, Z.-Y., and Song, W.-H.: Isotope-based source apportionment of nitrogen-containing aerosols: A case study in an industrial city in China, *Atmospheric Environment*, 212, 96-105, 10.1016/j.atmosenv.2019.05.020, 2019.
- Fan, M. Y., Zhang, Y. L., Lin, Y. C., Cao, F., Zhao, Z. Y., Sun, Y., Qiu, Y., Fu, P., and Wang, Y.: Changes of Emission Sources to Nitrate Aerosols in Beijing After the Clean Air Actions: Evidence From Dual Isotope Compositions, *Journal of Geophysical Research: Atmospheres*, 125, 10.1029/2019jd031998, 2020.
- 365 Fang, Y. T., Koba, K., Wang, X. M., Wen, D. Z., Li, J., Takebayashi, Y., Liu, X. Y., and Yoh, M.: Anthropogenic imprints on nitrogen and oxygen isotopic composition of precipitation nitrate in a nitrogen-polluted city in southern China, *Atmospheric Chemistry and Physics*, 11, 1313-1325, 10.5194/acp-11-1313-2011, 2011.
- Felix, J. D. and Elliott, E. M.: Isotopic composition of passively collected nitrogen dioxide emissions: Vehicle, soil and livestock source signatures, *Atmospheric Environment*, 92, 359-366, 10.1016/j.atmosenv.2014.04.005, 2014.
- 370 Felix, J. D., Elliott, E. M., and Shaw, S. L.: Nitrogen isotopic composition of coal-fired power plant NO_x : influence of emission controls and implications for global emission inventories, *Environ Sci Technol*, 46, 3528-3535, 10.1021/es203355v, 2012.
- Felix, J. D., Elliott, E. M., Gish, T., Maghirang, R., Cambal, L., and Clougherty, J.: Examining the transport of ammonia emissions across landscapes using nitrogen isotope ratios, *Atmospheric Environment*, 95, 563-570, 10.1016/j.atmosenv.2014.06.061, 2014.



- 375 Gobel, A. R., Altieri, K. E., Peters, A. J., Hastings, M. G., and Sigman, D. M.: Insights into anthropogenic nitrogen deposition to the North Atlantic investigated using the isotopic composition of aerosol and rainwater nitrate, *Geophysical Research Letters*, 40, 5977-5982, 10.1002/2013gl058167, 2013.
- Guha, T., Lin, C. T., Bhattacharya, S. K., Mahajan, A. S., Ou-Yang, C.-F., Lan, Y.-P., Hsu, S. C., and Liang, M.-C.: Isotopic ratios of nitrate in aerosol samples from Mt. Lulin, a high-altitude station in Central Taiwan, *Atmospheric Environment*, 154, 53-69, 10.1016/j.atmosenv.2017.01.036, 2017.
- 380 Hastings, M. G., Sigman, D. M., and Lipschultz, F.: Isotopic evidence for source changes of nitrate in rain at Bermuda, *Journal of Geophysical Research: Atmospheres*, 108, n/a-n/a, 10.1029/2003jd003789, 2003.
- Hoffman, R. C., Laskin, A., and Finlayson-Pitts, B. J.: Sodium nitrate particles: physical and chemical properties during hydration and dehydration, and implications for aged sea salt aerosols, *Journal of Aerosol Science*, 35, 869-887, 10.1016/j.jaerosci.2004.02.003, 2004.
- 385 Hsieh, M.-K.: Effects of orographically induced low-level moisture convergence and inversion strength on upslope fog: a case study at Xitou, Graduate Institute of Atmospheric Sciences, National Taiwan University, Taipei, Taiwan, 10.6342/NTU201900872, 2019.
- Huang, R.-T.: A study of aerosol hygroscopicity in Kinmen, Graduate Institute of Atmospheric Sciences, National Taiwan University, Taipei, Taiwan, 10.6342/NTU201603559, 2016.
- 390 Hung, H.-M., Hsu, C.-H., Lin, W.-T., and Chen, Y.-Q.: A case study of single hygroscopicity parameter and its link to the functional groups and phase transition for urban aerosols in Taipei City, *Atmospheric Environment*, 132, 240-248, 10.1016/j.atmosenv.2016.03.008, 2016.
- Jacob, D. J.: *Introduction to atmospheric chemistry*, Princeton University Press 1999.
- 395 Kawashima, H.: Seasonal trends of the stable nitrogen isotope ratio in particulate nitrogen compounds and their gaseous precursors in Akita, Japan, *Tellus B: Chemical and Physical Meteorology*, 71, 10.1080/16000889.2019.1627846, 2019.
- Kim, H., Park, G.-H., Lee, S.-E., Kim, Y.-i., Lee, K., Kim, Y.-H., and Kim, T.-W.: Stable isotope ratio of atmospheric and seawater nitrate in the East Sea in the northwestern Pacific ocean, *Marine Pollution Bulletin*, 149, 10.1016/j.marpolbul.2019.110610, 2019.
- 400 Pan, Y., Tian, S., Liu, D., Fang, Y., Zhu, X., Gao, M., Gao, J., Michalski, G., and Wang, Y.: Isotopic evidence for enhanced fossil fuel sources of aerosol ammonium in the urban atmosphere, *Environ Pollut*, 238, 942-947, 10.1016/j.envpol.2018.03.038, 2018a.
- Pan, Y., Tian, S., Liu, D., Fang, Y., Zhu, X., Zhang, Q., Zheng, B., Michalski, G., and Wang, Y.: Fossil Fuel Combustion-Related Emissions Dominate Atmospheric Ammonia Sources during Severe Haze Episodes: Evidence from (15)N-Stable Isotope in Size-Resolved Aerosol Ammonium, *Environ Sci Technol*, 50, 8049-8056, 10.1021/acs.est.6b00634, 2016.
- 405 Pan, Y., Tian, S., Liu, D., Fang, Y., Zhu, X., Gao, M., Wentworth, G. R., Michalski, G., Huang, X., and Wang, Y.: Source Apportionment of Aerosol Ammonium in an Ammonia-Rich Atmosphere: An Isotopic Study of Summer Clean and Hazy Days in Urban Beijing, *Journal of Geophysical Research: Atmospheres*, 123, 5681-5689, 10.1029/2017jd028095, 2018b.



- Petters, M. D. and Kreidenweis, S. M.: A single parameter representation of hygroscopic growth and cloud condensation
410 nucleus activity, *Atmospheric Chemistry and Physics*, 7, 1961-1971, 10.5194/acp-7-1961-2007, 2007.
- Poschl, U.: Atmospheric aerosols: composition, transformation, climate and health effects, *Angewandte Chemie International
Edition*, 44, 7520-7540, 10.1002/anie.200501122, 2005.
- Savard, M. M., Cole, A., Smirnoff, A., and Vet, R.: $\delta^{15}\text{N}$ values of atmospheric N species simultaneously collected using
sector-based samplers distant from sources – Isotopic inheritance and fractionation, *Atmospheric Environment*, 162, 11-22,
415 10.1016/j.atmosenv.2017.05.010, 2017.
- Savarino, J., Kaiser, J., Morin, S., Sigman, D. M., and Thiemens, M. H.: Nitrogen and oxygen isotopic constraints on the origin
of atmospheric nitrate in coastal Antarctica, *Atmospheric Chemistry and Physics*, 7, 1925-1945, 10.5194/acp-7-1925-2007,
2007.
- Seinfeld, J. H. and Pandis, S. N.: *Atmospheric Chemistry and Physics: From Air Pollution to Climate Change*, 2nd, John Wiley
420 & Sons, Inc.2006.
- Sigman, D. M., Casciotti, K. L., Andreani, M., Barford, C., Galanter, M., and Böhlke, J. K.: A Bacterial Method for the
Nitrogen Isotopic Analysis of Nitrate in Seawater and Freshwater, *Analytical Chemistry*, 73, 4145-4153, 10.1021/ac010088e,
2001.
- Stock, B. C., Jackson, A. L., Ward, E. J., Parnell, A. C., Phillips, D. L., and Semmens, B. X.: Analyzing mixing systems using
425 a new generation of Bayesian tracer mixing models, *PeerJ*, 6, e5096, 10.7717/peerj.5096, 2018.
- Sun, X., Zong, Z., Wang, K., Li, B., Fu, D., Shi, X., Tang, B., Lu, L., Thapa, S., Qi, H., and Tian, C.: The importance of coal
combustion and heterogeneous reaction for atmospheric nitrate pollution in a cold metropolis in China: Insights from isotope
fractionation and Bayesian mixing model, *Atmospheric Environment*, 243, 10.1016/j.atmosenv.2020.117730, 2020.
- Walters, W. W. and Michalski, G.: Theoretical calculation of nitrogen isotope equilibrium exchange fractionation factors for
430 various NO_y molecules, *Geochimica et Cosmochimica Acta*, 164, 284-297, 10.1016/j.gca.2015.05.029, 2015.
- Walters, W. W., Chai, J., and Hastings, M. G.: Theoretical Phase Resolved Ammonia–Ammonium Nitrogen Equilibrium
Isotope Exchange Fractionations: Applications for Tracking Atmospheric Ammonia Gas-to-Particle Conversion, *ACS Earth
and Space Chemistry*, 3, 79-89, 10.1021/acsearthspacechem.8b00140, 2018.
- Walters, W. W., Tharp, B. D., Fang, H., Kozak, B. J., and Michalski, G.: Nitrogen Isotope Composition of Thermally Produced
435 NO_x from Various Fossil-Fuel Combustion Sources, *Environ Sci Technol*, 49, 11363-11371, 10.1021/acs.est.5b02769, 2015.
- Wankel, S. D., Chen, Y., Kendall, C., Post, A. F., and Paytan, A.: Sources of aerosol nitrate to the Gulf of Aqaba: Evidence
from $\delta^{15}\text{N}$ and $\delta^{18}\text{O}$ of nitrate and trace metal chemistry, *Marine Chemistry*, 120, 90-99, 10.1016/j.marchem.2009.01.013,
2010.
- Weigand, M. A., Foriel, J., Barnett, B., Oleynik, S., and Sigman, D. M.: Updates to instrumentation and protocols for isotopic
440 analysis of nitrate by the denitrifier method, *Rapid Commun Mass Spectrom*, 30, 1365-1383, 10.1002/rcm.7570, 2016.



Zhang, Z., Zeng, Y., Zheng, N., Luo, L., Xiao, H., and Xiao, H.: Fossil fuel-related emissions were the major source of NH₃ pollution in urban cities of northern China in the autumn of 2017, *Environ Pollut*, 256, 113428, 10.1016/j.envpol.2019.113428, 2020.



Tables

Table 1. IR measured functional group average concentration of collected PM₁₀ under different weather conditions. (mean, [min, max] at the unit of µg/m³)

	Overall	non-foggy daytime	foggy daytime	non-foggy nighttime	foggy nighttime
NH₄⁺	0.98, [0.15, 3.31]	1.00	2.48	0.56	1.12
NO₃⁻	0.25, [0.00, 1.51]	0.25	0.92	0.04	0.34
SO₄²⁻	5.16, [0.62, 12.97]	5.62	10.14	3.58	5.01
BC	0.81, [0.48, 1.46]	0.95	1.25	0.59	0.71



450 **Table 2. Aerosol $\delta^{15}\text{N}$ values of different sources used in this study. (Savard et al., 2017)**

NH_4^+ source	NH_4^+ $\delta^{15}\text{N}$ (mean \pm SD)	NO_3^- source	NO_3^- $\delta^{15}\text{N}$ (mean \pm SD)
CFPP	3.4 \pm 10.4	CFPP	6.1 \pm 2.0
traffic	17.1 \pm 9.1	urban	5.7 \pm 2.0
chemical and metal industries	11.0 \pm 2.4	chemical and metal industries	1.0 \pm 4.7
fertilizers plus oil	16.3	fertilizers plus oil	10.8
feedlots	27.7 \pm 7.0		



Table 3. Mass-weighted isotope value (‰) and probable single source under distinct weather circumstances.

	Non-foggy daytime	Foggy daytime	Non-foggy nighttime	Foggy nighttime
$\delta^{15}\text{N}$ of NH_4^+ (probable sources)	13.20 (CFPP, traffic, industries)	15.52 (traffic)	9.30 (CFPP, traffic, industries)	13.33 (CFPP, traffic, industries)
$\delta^{15}\text{N}$ of $\text{PM}_1\text{-NO}_3^-$ (probable sources)	-	1.70 (industries)	-	1.46 (industries)
$\delta^{15}\text{N}$ of $\text{PM}_{1-10}\text{-NO}_3^-$ (probable sources)	2.72 (industries)	3.98 (urban, industries)	1.85 (industries)	-
$\delta^{18}\text{O}$ of $\text{PM}_1\text{-NO}_3^-$	-	70.48	-	79.81
$\delta^{18}\text{O}$ of $\text{PM}_{1-10}\text{-NO}_3^-$	70.05	71.62	74.82	-

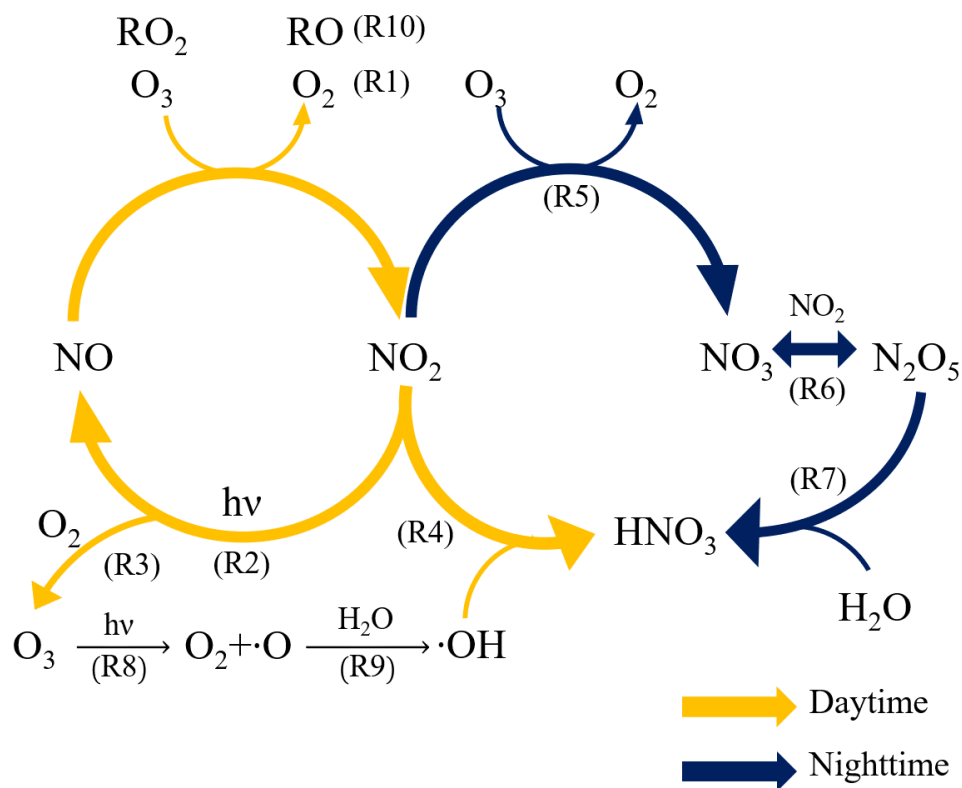


Table 4. The posterior probabilities of aerosol sources inferred by MixSIAR (starred for the mean posterior probability greater than 20%.)

Weather condition (sample size, n)	NH ₄ ⁺ sources and posterior probabilities (Mean ± SD, %)				
	CFPP	industries	feedlots	fertilizers	traffic
all cases (10)	25.7 ± 15.1*	32.5 ± 22.0*	9.2 ± 8.2	17.7 ± 14.3	15.0 ± 13.5
non-foggy day (3)	19.0 ± 14.6	28.5 ± 20.0*	13.8 ± 12.0	22.1 ± 17.4*	16.6 ± 14.1
foggy day (2)	13.9 ± 12.5	24.2 ± 17.9*	17.0 ± 13.6	27.2 ± 20.9*	17.7 ± 14.8
non-foggy night (4)	21.0 ± 14.7*	32.3 ± 21.2*	10.6 ± 9.8	20.5 ± 16.4*	15.5 ± 13.4
foggy night (1)	19.1 ± 15.0	23.1 ± 17.9*	17.3 ± 14.3	20.5 ± 17.0*	20.0 ± 15.9*
PM₁₋₁₀-NO₃⁻ sources					
	CFPP	industries	fertilizers	urban	
all cases (5)	27.2 ± 19.3*	30.7 ± 17.8*	13.9 ± 12.2	28.2 ± 19.8*	
non-foggy day (2)	27.8 ± 19.7*	25.2 ± 18.0*	19.7 ± 15.6	27.4 ± 20.3*	
foggy day (2)	28.0 ± 19.9*	25.3 ± 17.3*	19.2 ± 15.4	27.6 ± 19.4*	
non-foggy night (1)	26.5 ± 20.5*	27.2 ± 19.6*	19.8 ± 16.2	26.5 ± 20.0*	
PM₁-NO₃⁻ sources					
	CFPP	industries	fertilizers	urban	
all cases (3)	23.8 ± 18.2*	36.5 ± 21.0*	14.6 ± 13.3	25.1 ± 19.2*	
foggy day (2)	26.6 ± 19.9*	30.0 ± 19.4*	16.6 ± 14.8	26.7 ± 19.7*	
foggy night (1)	27.4 ± 19.9*	26.9 ± 19.3*	19.1 ± 15.8	26.6 ± 19.7*	

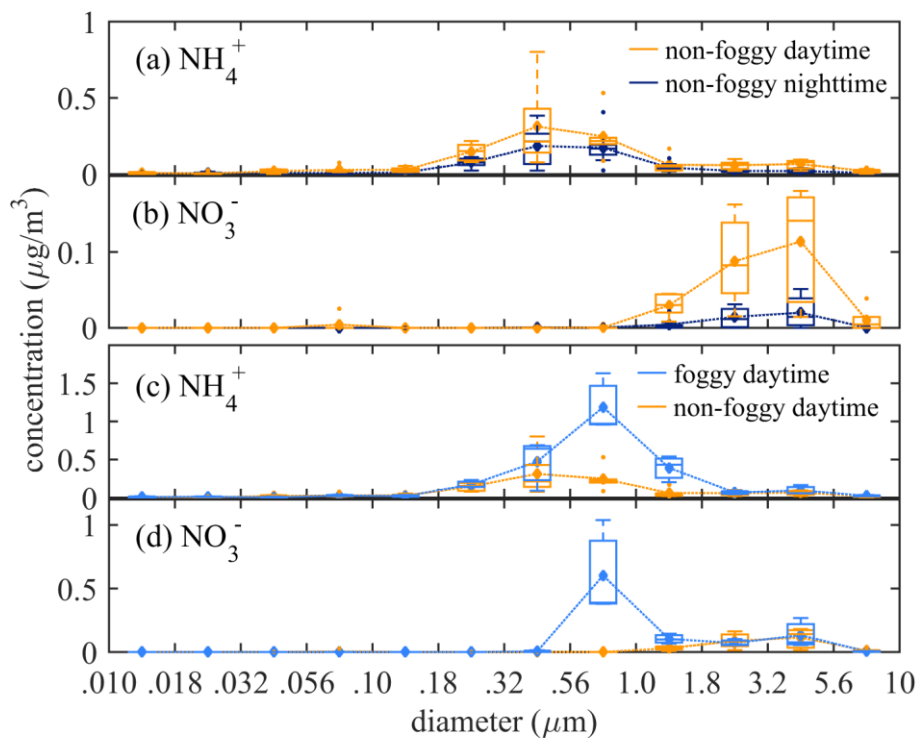


Figures



460

Figure 1: The formation pathway of nitric acid to form aerosol nitrate during daytime and nighttime.



465 **Figure 2:** The statistical box plot of concentrations as a function of size bin at non-foggy daytime and nighttime for (a) NH_4^+ , and (b) NO_3^- , and at foggy and non-foggy daytime for (c) NH_4^+ and (d) NO_3^- . (diamond: mean value; outliers: $< 1^{\text{st}}$ quartile $Q1-1.5$ interquartile range (IQR) or $> 3^{\text{rd}}$ quartile $Q3+1.5$ IQR).

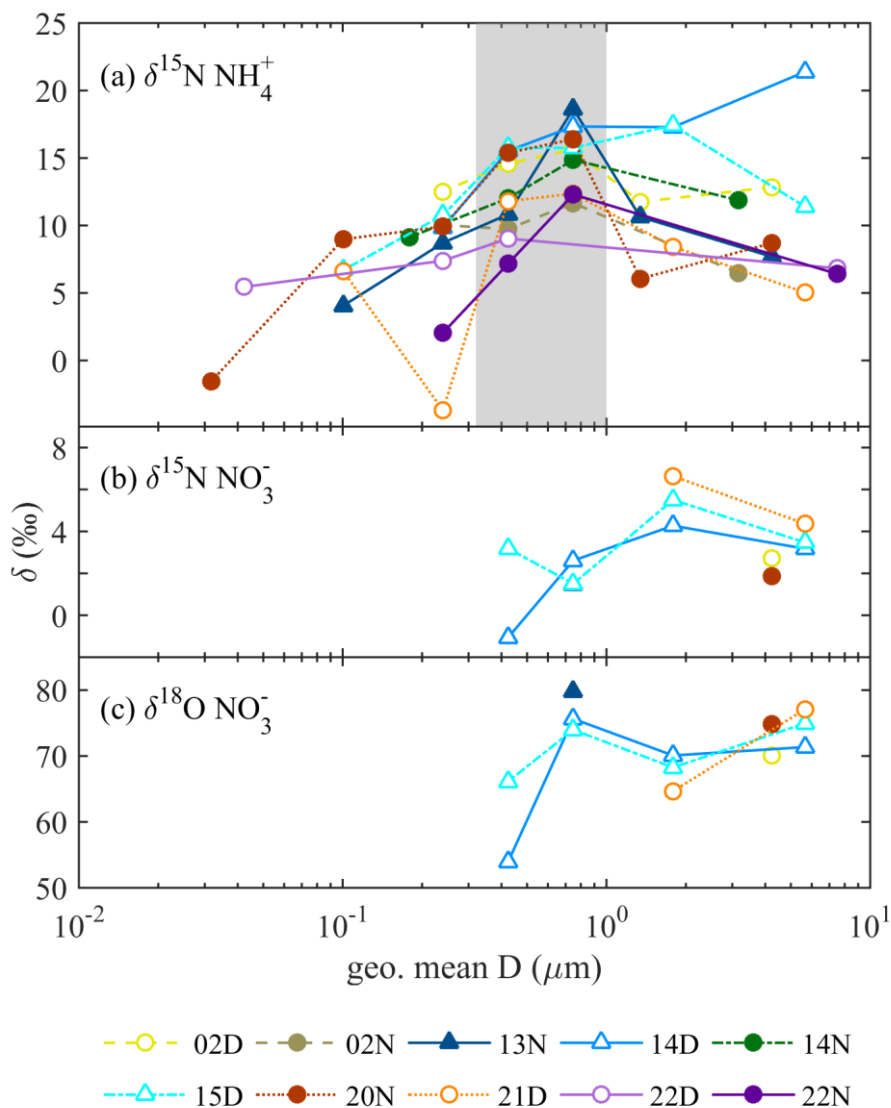
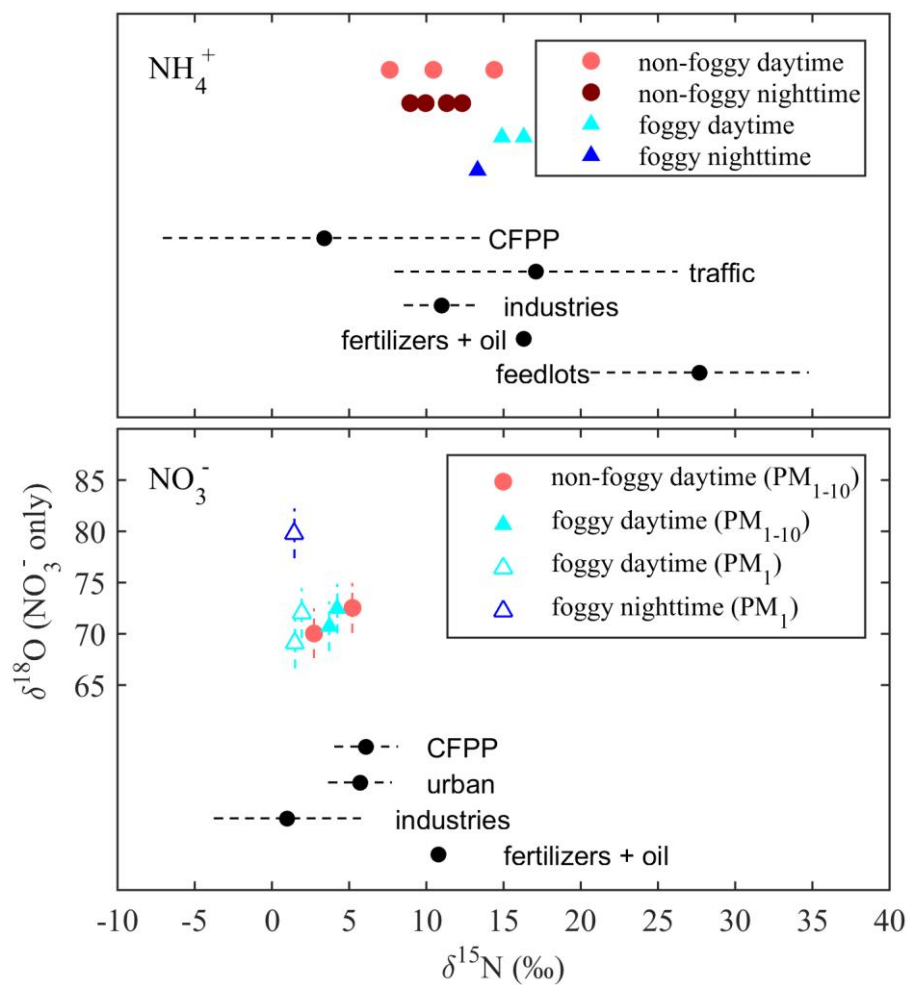


Figure 3: The isotope values as a function of collected aerosol geometric mean diameter (D) (a) δ¹⁵N NH₄⁺, (b) δ¹⁵N NO₃⁻, and (c) δ¹⁸O NO₃⁻. The symbol is hollow for daytime, filled for nighttime, and triangle for foggy events, respectively.



470 **Figure 4:** Comparison between the period mass-averaged isotope values ($\delta^{15}\text{N}$ and $\delta^{18}\text{O}$) and the mean $\delta^{15}\text{N}$ value (black dots) by Savard et al. (2017) for different sources. The dashed lines are the standard deviation of the measurements. The batch SD of international standards' duplicates was 0.04 - 0.11‰ for $\delta^{15}\text{N}$ (not observable in this figure), and 2.20 - 2.33‰ for $\delta^{18}\text{O}$ as shown at each data point.